J. Phys.: Condens. Matter **20** (2008) 255213 (7pp) doi:10.1088/0953-8984/20/25/255213

A Mössbauer spectroscopy investigation of h-$YbMnO_3$

Hazar A Salama[1], G A Stewart[1], D H Ryan[2], M Elouneg-Jamroz[2] and A V J Edge[1]

[1] School of Physical, Environmental and Mathematical Sciences, University of New South Wales at the Australian Defence Force Academy, Canberra 2600, Australia
[2] Centre for the Physics of Materials and Physics Department, McGill University, Montreal, QC, H3A 2T8, Canada

Received 7 March 2008, in final form 24 April 2008
Published 21 May 2008
Online at stacks.iop.org/JPhysCM/20/255213

Abstract

^{170}Yb and ^{57}Fe Mössbauer spectra are reported for hexagonal phase $YbMnO_3$ and $Yb(^{57}Fe_xMn_{1-x})O_3$ ($x = 0.005, 0.01$), respectively. The dilute concentrations of ^{57}Fe are demonstrated to provide a reliable, non-perturbing Mössbauer spectroscopy probe of the Mn sub-lattice magnetization. Substitution of up to 1 at.% ^{57}Fe exerts negligible influence on the Néel temperature ($T_{N_1} \approx 88$–89 K) and point charge model estimates of the electric field gradient agree well with experimental ^{57}Fe Mössbauer results in terms of both sign and magnitude. The ^{170}Yb Mössbauer spectrum recorded at 4.5 K provides support for strong crystal field quenching with isolated Kramers doublet ground states at both Yb sites. A 'static', five-line sub-spectrum is tentatively assigned to the 4b site, for which the slowed fluctuation of the Kramers doublet is attributed to non-zero magnetic exchange with the antiferromagnetic Mn sub-lattice. This is not the case for the 2a site whose sub-spectrum is a motionally narrowed single line. On the basis of this work, the saturation magnetization for the ordered Yb sub-lattice ($T_{N_2} \leqslant 3$ K) is estimated at $\approx 1.8\ \mu_B$ per formula unit, in close agreement with single-crystal magnetization data reported elsewhere.

(Some figures in this article are in colour only in the electronic version)

1. Introduction

The heavier rare earth manganites, $RMnO_3$ (R = Y, Ho → Lu), crystallize in the hexagonal $LnMnO_3$-type structure with the space group $P6_3cm$. There is one manganese site (6c) and two rare earth sites (2a and 4b) [1–3]. These manganites are currently of interest because they undergo both a ferroelectric transition at $T_C \approx 1000$ K and an antiferromagnetic transition at a lower temperature ($T_{N_1} \approx 100$ K) due to strong couplings between the Mn^{3+} moments. In addition, the Mn ions form a corner-sharing triangular network which leads to geometrical frustration [4]. Using conventional bulk magnetization methods, the Néel temperature for $YbMnO_3$ has been reported in the literature as 82 K [5] for a single-crystal specimen and 88 K [6, 7] for powdered specimens. A recent infra-red absorption study of single-crystal $YbMnO_3$ reported a Néel temperature of 75 K [8]. This was determined by monitoring the exchange splitting of the Yb^{3+} 4b site, crystal field (CF) levels as a function of temperature.

In this present work, we have employed ^{57}Fe Mössbauer spectroscopy to probe the Mn sub-lattice magnetization of $YbMnO_3$ as a function of temperature. To that end, the Mn sub-lattice has been doped with dilute concentrations (0.5 and 1.0 at.%) of enriched ^{57}Fe. In addition, ^{170}Yb Mössbauer spectroscopy at 4.5 K has been used to investigate the magnetic behaviour of the Yb^{3+} ions already present as a stoichiometric component of the compound.

2. Experimental details

Specimens of $YbFe_xMn_{1-x}O_3$ ($x = 0$, 0.05, 0.01) were prepared from stoichiometric amounts of Yb_2O_3 (99.9%), Fe_2O_3 (99+%) and $MnCO_3$ (99.9%). The Fe_2O_3 employed was enriched to 96 at.% ^{57}Fe (compared with the natural isotopic abundance of just 2.2 at.%). Given that Yb_2O_3 absorbs CO_2 from the atmosphere, it was heated in air at 500 °C for 1 h prior to weighing. The materials were then mixed intimately using a mortar and pestle, pressed into a pill, and heated in air

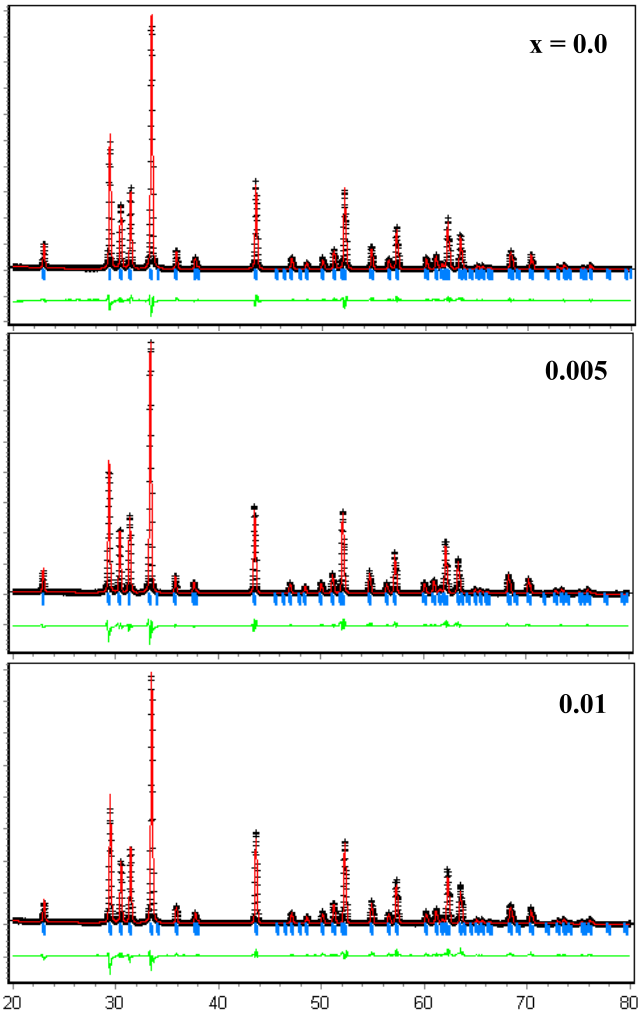

Figure 1. X-ray powder diffraction patterns for Yb(^{57}Fe$_x$Mn$_{1-x}$)O$_3$ with $x = 0$, 0.005 and 0.01.

at 1250 °C for 16 h. This process was repeated three times. For the first heat treatment cycle, the temperature was held at 900 °C for 1 h before proceeding to 1250 °C. The purpose of this was to allow the expelled CO_2 to diffuse gently out of the pellet.

X-ray powder diffraction patterns (figure 1) recorded using Cu Kα radiation were consistent with a single hexagonal phase for all three specimens. The solid curves drawn through the data in figure 1 were fitted using *Rietica* [9]. The fitted lattice parameters are given in table 1. The change brought about by the Fe substitution is relatively minor, although the unit cell volume is some 0.2% less for $x = 0.01$ than for the lower concentrations and there is a worsening of the quality of the fit (increasing profile residual, R_p) as x increases. The lattice parameter values derived for pure $YbMnO_3$ lie at the mean of the sets of parameters reported by van Aken *et al* [2, 3], Katsufuji *et al* [5] and Zhou *et al* [10].

A *Quantum Design* PPMS susceptometer was used to measure the AC magnetization data for a 500 mg specimen of pure host material. The best results were achieved in zero applied field with a frequency of 10 kHz and $B_{AC}(\max) = 0.1$ mT.

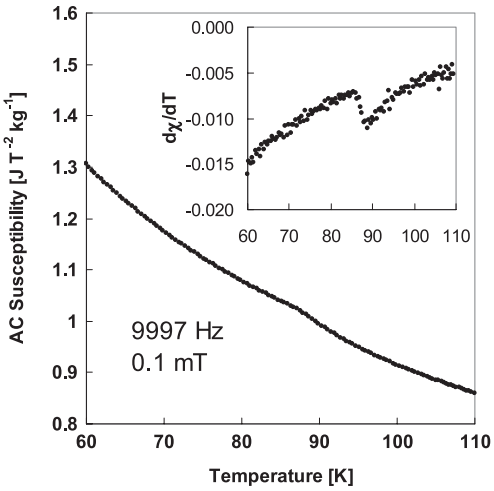

Figure 2. Temperature dependence of the AC magnetic susceptibility, χ, at low temperatures in zero external field. The inset shows the $d\chi/dT$ as a function of temperature.

Table 1. Lattice parameters, cell volumes, profile residuals for the *Rietica* analyses, and Mn sub-lattice ordering temperatures, T_{N_1} (χ_{AC} = AC susceptibility; MS = ^{57}Fe Mössbauer spectroscopy) for Yb(^{57}Fe$_x$Mn$_{1-x}$)O$_3$ with $x = 0$, 0.005 and 0.01.

x	a (nm)	c (nm)	V (nm^3)	R_p	T_{N_1} (K)
0	0.6062(1)	1.1371(1)	0.3619(2)	8.7	88 (χ_{AC})
0.005	0.6064(1)	1.1367(1)	0.3620(2)	7.7	$\leqslant$88(MS)
0.01	0.6056(1)	1.1369(1)	0.3611(2)	9.2	$\geqslant$89(MS)

The ^{57}Fe Mössbauer spectra were recorded for sample absorber temperatures over the range 4.2–300 K using a commercial ^{57}Co:Rh source mounted outside the cryostat at room temperature and a Kr(CO_2) gas proportional counter. The absorbers were comprised of $\approx$10 mg cm^{-2} of specimen material diluted with CB_4. For ^{170}Yb Mössbauer spectrum acquisition, both the source and absorber ($\approx$600 mg cm^{-2}) were mounted vertically inside a helium-flow cryostat at 4.5 K. The 20 mCi ^{170}Tm source was prepared by neutron activation of $\approx$25 mg of Tm as a 10 wt% alloy in aluminium. The 84.25 keV γ-photons were resolved from the various x-rays emitted by the source using a high purity Ge detector. Both drives were oscillated in sine mode. In the ^{57}Fe Mössbauer case, the drive velocity was calibrated against the spectrum for α-Fe. The ^{170}Yb Mössbauer drive velocity was calibrated using a laser interferometer mounted on the back of the drive.

3. Results and discussion

The AC magnetic susceptibility data, recorded with a high density of data points over the temperature range 60–110 K, are presented in figure 2. There is a small feature associated with the Néel temperature at $T_{N_1} = 88$ K which is more evident in the plot of the temperature derivative (inset in figure 2). These data bear a close resemblance to the DC magnetization data of Huang *et al* [7] and the Néel temperatures are in excellent agreement.

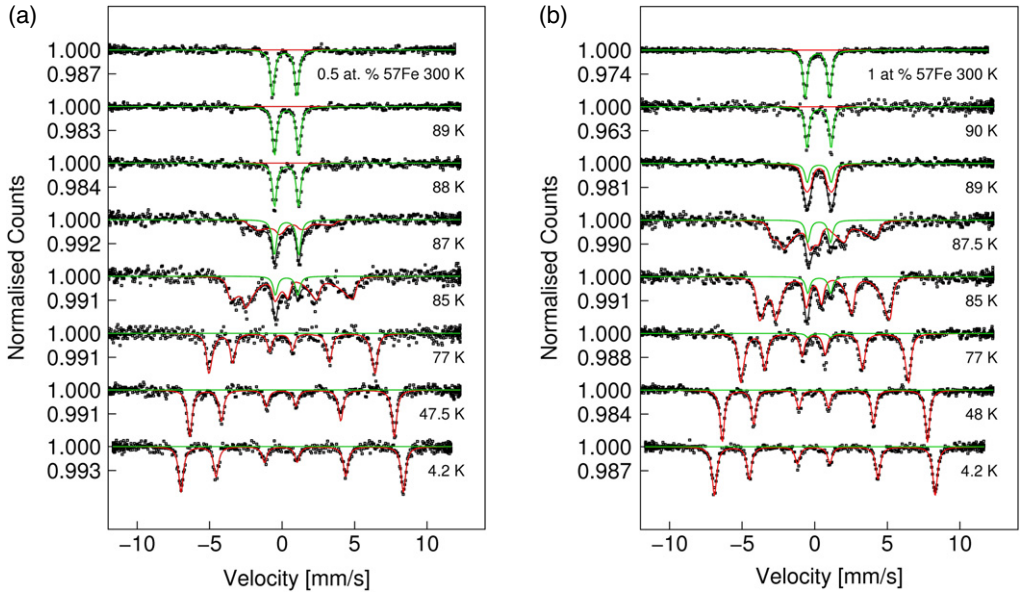

Figure 3. Temperature-dependent ^{57}Fe Mössbauer spectra of Yb(^{57}Fe$_x$Mn$_{1-x}$)O$_3$ with (a) $x = 0.005$ and (b) $x = 0.01$.

Table 2. Experimental results for (a) ^{57}Fe Mössbauer and (b) ^{170}Yb Mössbauer spectroscopy investigations of hexagonal Yb(^{57}Fe$_x$Mn$_{1-x}$)O$_3$. The isomer shift, δ, is given relative to α-Fe (for ^{57}Fe) and ^{170}Yb:Tm(10 wt%)Al (for ^{170}Yb). θ is the orientation of the magnetic hyperfine field $B_{\rm hf}$ with respect to the principal z-axis of the electric field gradient tensor. Various point charge model (PCM) and crystal field (CF) theory estimates for $B_{\rm hf}$ and the quadrupole interaction strength, eQV_{zz}, are included for comparison.

	T (K)	x	δ (mm s^{-1})	Γ (mm s^{-1})	eQV_{zz} (mm s^{-1})	$B_{\rm hf}$ (T)	θ (deg)
			^{57}Fe Mössbauer				
PCM					−3.36(16)		
Expt	295	0.005	+0.292(3)	0.34(2)	−3.36(2)		
		0.01	+0.296(2)	0.35(1)	−3.34(2)		
	4.2	0.005	+0.420(7)	0.39(2)	−3.20(2)	47.07(3)	90
		0.01	+0.421(3)	0.38(2)	−3.14(2)	46.67(2)	90
			^{170}Yb Mössbauer				
Free ion					+55.7	412.5	
CF (4b site)					<3.5	183.2	
Expt ('static')	4.5	0	+0.012(1)	3.2(1)	1.68(1)	173.5(1)	

The ^{57}Fe Mössbauer spectra for $x = 0.005$ and 0.01 are presented as a function of temperature in figures 3(a) and (b), respectively. At the extremes of the temperature range, the Mössbauer spectra are relatively straightforward. The room temperature Mössbauer spectrum is a single doublet corresponding to the paramagnetic phase. At 4.2 K, the spectrum is a single magnetically split sextet corresponding to the magnetic phase. The fit parameters for the room temperature and 4.2 K spectra are summarized in table 2. In order to achieve similar values of the quadrupole interaction strength eQV_{zz} at the two temperatures, it was necessary to set the magnetic hyperfine field $B_{\rm hf}$ perpendicular ($\theta = 90°$) to the z-axis of the electric field gradient and employ a full analysis of the mixed magnetic/quadrupole hyperfine interaction. The 4.2 K values of $B_{\rm hf} = 47.1$ T ($x = 0.005$) and 46.7 T ($x = 0.01$) are typical for the high spin $S = 5/2$ state of Fe^{3+}. For example, similar saturated fields were observed for ^{57}Fe probes in the green phase cuprate Gd_2BaCuO_5 [11].

In the intermediate temperature range, the magnetic spectra are seen to collapse with increasing temperature (figure 3). As the temperature approaches T_{N_1}, the magnetic sextet becomes increasingly broadened and coexists with an increasingly intense paramagnetic doublet. The line broadening is asymmetric. This can often be attributed to a $B_{\rm hf}$ distribution caused by variation in the number of nearest neighbours that are also ^{57}Fe. However, for the specimens considered here, the ^{57}Fe concentrations are very small and there is no evidence of asymmetric line broadening at 4.2 K. It is more likely that this is a relaxation effect. Similar relaxation spectra were observed for dilute ^{57}Fe probes in the generic $La_{2/3}Ca_{1/3}MnO_3$ [12]. On the basis of a close similarity of the asymmetric line broadenings observed for the present spectra and for spectra reported elsewhere for iron oxides [13, 14], we employed the same slow relaxation analysis model as those authors. The fitted theory curves are shown in figure 3 and the maximum $B_{\rm hf}$ values are presented as a function of temperature

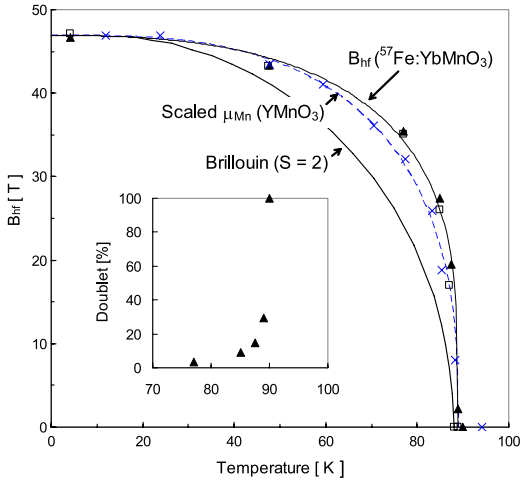

Figure 4. Temperature dependence of the ^{57}Fe hyperfine field, B_{hf}, for Yb(^{57}Fe$_x$Mn$_{1-x}$)O$_3$ with $x = 0.005$ (open squares) and 0.01 (solid triangles). The solid line is a fit of the empirical formula (equation (1)) to the experimental data with $\alpha = 2.6$ and $\beta = 0.27$. Also included are the Brillouin curve for $S = 2$ (dotted line) and the μ(Mn) data for YMnO$_3$ ([15]) which have been scaled to the same saturation value and ordering temperature (crosses and broken curve). The temperature dependence of the paramagnetic doublet intensity is shown in the inset for $x = 0.01$.

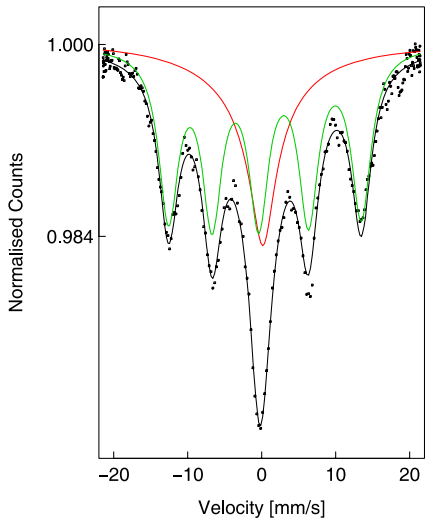

Figure 5. ^{170}Yb Mössbauer spectrum for YbMnO$_3$ at 4.5 K. The fitted theory curve is comprised of a 'static' five-line magnetic sub-spectrum (green on-line) and a motionally narrowed, single-line sub-spectrum (red on-line) that corresponds to a rapidly fluctuating, well-isolated, Kramers doublet.

in figure 4. The variation of the relative paramagnetic doublet intensity is shown in the inset of figure 4 for $x = 0.01$.

From the appearance of the ^{57}Fe Mössbauer spectra and the temperature dependence of B_{hf} at the ^{57}Fe probe, it is concluded that the ^{57}Fe-doped specimens order at $\leqslant$88 K ($x = 0.005$) and $\geqslant$89 K ($x = 0.01$) where the uncertainty is of the order of $\pm$0.3 K. The two values are included in the final column of table 1. It is possible that there is a genuine increase induced by the additional ^{57}Fe content but it is small compared with the range of ordering temperatures reported elsewhere in the literature. The temperatures are in close agreement with the magnetic susceptibility determination of $T_{N_l} = 88$ K for the pure host material. It is intriguing that the Néel temperatures determined here are similar to previous determinations for polycrystalline specimens [6, 7] but significantly higher than the values of 82 K [5] and 75 K [8] determined for single-crystal specimens (it may yet prove to be significant that the paramagnetic doublet component of ^{57}Fe Mössbauer spectra approaches zero intensity in the latter temperature range). The temperature dependence of B_{hf} has the general appearance of a molecular field theory curve but is more closely represented by an empirical relationship (solid theory curve in figure 4) of the form

$$B_{hf} = B_{hf}(T = 0)\left(1 - \left(\frac{T}{T_N}\right)^{\alpha}\right)^{\beta} \qquad (1)$$

with $\alpha = 2.6$ and $\beta = 0.27$.

Neutron diffraction has been used on several occasions to determine the magnetic moment as a function of temperature for the Mn sub-lattice of YMnO$_3$ [15–17] and a scaled version of the set of data due to Park *et al* [15] is included in figure 4 for ease of comparison. It is evident that the Mn sub-lattice magnetization for pure YMnO$_3$ exhibits very similar temperature dependence to that of the present B_{hf} results for ^{57}Fe-doped YbMnO$_3$. This is supported by the fact that the empirical relationship parameters of $\alpha = 2.2(7)$ and $\beta = 0.34(8)$ derived for YMnO$_3$ (Lonkai [17]) compare favourably with those obtained above. On the basis of these observations, the dilute ^{57}Fe probes appear to behave as an integral component of the Mn sub-lattice. That is, the ^{57}Fe concentration has negligible influence on T_{N_l} and the local ^{57}Fe moment follows closely the expected temperature variation of the Mn magnetization.

The ^{170}Yb Mössbauer spectrum recorded for pure YbMnO$_3$ at 4.5 K is presented in figure 5. The best theoretical fit to the spectrum was achieved with a 'static', magnetically split, five-line sub-spectrum superimposed on a broad single-line sub-spectrum with relative intensities of 2:1. The quadrupole interaction is too small to justify a full analysis of the mixed magnetic/quadrupole hyperfine interaction for the 'static' sub-spectrum and a simple coaxial interaction was employed. For this reason it was not possible to determine the orientation of the magnetic hyperfine field with respect to the c-axis, and the fitted quadrupole interaction strength is a value 'projected' onto the direction of the hyperfine field. The fitted parameters for the 'static' sub-spectrum are included in table 2. The isomer shift, given with respect to the Tm(10 wt%)Al source, is negligible compared with the linewidth. At 3.2(1) mm s^{-1}, the linewidth, Γ, is larger than the value of 2.66(12) mm s^{-1} recorded with the same source and a standard specimen of YbB$_6$ but it is typical for ceramic materials of the type considered here. The magnetic hyperfine field value of 173.5(1) T and the quadrupole interaction strength of $eQV_{zz} = 1.68(1)$ mm s^{-1} are significantly smaller than the maximum possible Yb^{3+} 'free ion' values of 412.5 T and 55.7 mm s^{-1} [18], respectively. This implies strong CF quenching of the electronic angular momentum, consistent with the work of Diviš *et al* [8] who deduced well-isolated,

Kramers doublet ground states for the two Yb sites. It is likely, therefore, that the collapse to a broad, single-line sub-spectrum is due to rapid fluctuation of the Kramers doublet. Here, 'rapid' is to be taken as fast when compared with the rate of the ^{170}Yb nuclear magnetic moment's Larmor precession. As a useful reference, the 'static' sub-spectrum's fitted hyperfine field of 173.5 T corresponds to a precession time of $\approx 2 \times 10^{-9}$ s. For the purpose of the spectrum analysis, we employed the relaxation model of Wickman *et al* [20]. The relaxation time of the rapid spin fluctuations was determined as $\approx 6 \times 10^{-11}$ s. The fit was performed manually by a process of trial and error and it was difficult to assign an uncertainty to this parameter.

Similar low temperature spectra were observed by Hodges *et al* in their investigation of geometrically frustrated $Yb_2Ti_2O_7$ [19]. For that system there is only one Yb site and the presence of the 'static' sub-spectrum was attributed to a slowing down of the dynamics of short range correlated spins, associated with a first-order transition at 0.23 K. It is conceivable that a similar mechanism could come into play in $YbMnO_3$. The Yb sub-lattice is reported to order magnetically at $T_{N_2} \approx 3$ K [21], just below the spectrum acquisition temperature of 4.5 K. However, the ratio of the intensities (2:1) of the 'static' and single-line sub-spectra suggests that the 'static' sub-spectrum is associated with Yb^{3+} ions located at the more prevalent 4b site and the broad single-line sub-spectrum is associated with the 2a site. If this interpretation is correct, then the Kramers doublet's slower fluctuation rate at the Yb 4b site more probably has its origins in the antiferromagnetism of the Mn sub-lattice. It is generally assumed that the triangular spin arrangement of the local Mn moments results in a zero net molecular field at the rare earth sites. It is interesting, therefore, that Diviš *et al* [8] observed magnetic splitting of the IR transitions below T_{N_1}. However, this was just for the lower symmetry 4b site, a feature that they were able to use as a convenient label. Given that the Mn moments are directed perpendicular to the crystallographic *c*-axis, the influence of the molecular field arising from them would be to split the Kramers doublet and induce local moments in the basal plane, thereby slowing the fluctuation rate for the Yb^{3+} ions only at the 4b sites.

4. Point charge model and crystal field theory

The hexagonal $RMnO_3$ structure consists of MnO_5 bipyramids stacked in layers alternating with layers of R^{3+} ions.

4.1. The Mn site

Each Mn^{3+} ion is surrounded by three in-plane and two apical oxygen ions (figure 6). Strictly, the Mn 4c site has monoclinic *m* (C_S) point symmetry which is consistent with an asymmetric electric field gradient tensor ($\eta_{\text{latt}} \neq 0$). However, the local bipyramidal environment is well approximated by trigonal symmetry and a point charge model (PCM) summation over the five nearest O^{2-} neighbours yields $V_{zz} \approx -7.68 \times 10^{21}$ V m^{-2} and $\eta = 0.01 \approx 0$ with respect to axes x_{EFG}, $z_{\text{EFG}} \parallel a, c$. Given that the Fe^{3+} and Mn^{2+} ions are of comparable radius ($r^{3+}_{\text{Fe}} \approx r^{3+}_{\text{Mn}} \approx 0.58$ nm for fivefold

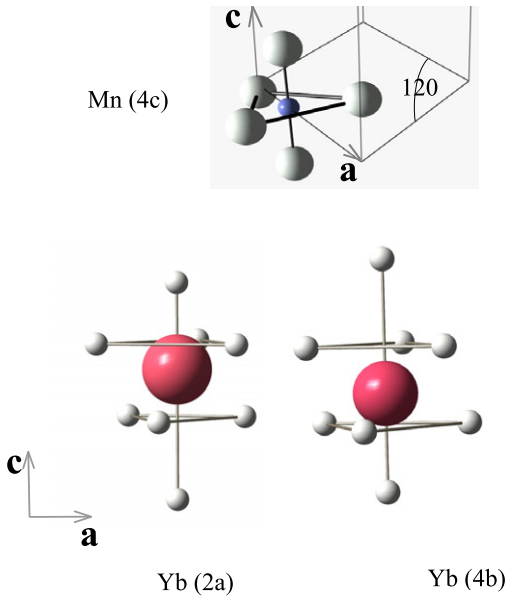

Figure 6. Mn and Yb site configurations for the hexagonal ($P6_3cm$) $YbMnO_3$ structure.

coordination [22]), it is reasonable to assume that the Mn site is not significantly distorted by Fe^{3+} substitution. Furthermore, Fe^{3+} is an S-state ion with a negligible 3d shell contribution to the electric field gradient at its nucleus. Adopting $Q(I = 3/2) = +0.21(1)$ b, $(1 - \gamma_\infty) = 10$ and $E\gamma = 14.412$ keV, the quadrupole interaction strength acting at the ^{57}Fe probe nuclei is then estimated at $eQV_{zz} = -3.36(16)$ mm s^{-1}. This estimate is included in table 2 where it is seen to be in excellent agreement (both sign and magnitude) with the experimental quadrupole interaction strength determined by ^{57}Fe Mössbauer spectroscopy. As mentioned in section 3, the best fits to the low temperature Mössbauer spectra were achieved with B_{hf} perpendicular to z_{EFG} where z_{EFG} is parallel to the *c*-axis according to the above PCM calculation. This confirms that the triangulated Mn sub-lattice magnetization lies in the basal plane, as determined elsewhere by Fiebig *et al* [23].

4.2. The ytterbium sites

The near-neighbour oxygen environments for the Yb 2a and 4b sites are also shown in figure 6. Diviš *et al* [8] analysed their IR absorption spectra for single-crystal h-$YbMnO_3$ and used a semi-empirical approach to arrive at preliminary sets of CF parameters for the two sites. The 2a and 4b sites have point symmetries 3*m* (C_{3v}) and 3 (C_3) respectively. However, given that the two local environments are very similar, it was assumed that the 4b site is also well approximated by the C_{3v} symmetry. In order to consider the influence of the CF splitting of the $^2F_{7/2}$ ground term on the ^{170}Yb Mössbauer spectrum, we have converted the results of Diviš *et al* [8] to the Stevens operator equivalent formalism ([24] and references therein) so that the CF Hamiltonian is then represented by

$$\mathcal{H}_{\text{CF}} = B_2^0 O_2^0 + B_4^0 O_4^0 + B_4^3 O_4^3 + B_6^0 O_6^0 + B_6^3 O_6^3 + B_6^6 O_6^6 \quad (2)$$

Table 3. Properties of the Yb^{3+} Kramers ground state doublets, $|\pm\rangle = \pm a|\mp\frac{5}{2}\rangle - b|\pm\frac{1}{2}\rangle \mp c|\pm\frac{7}{2}\rangle$, for the two Yb sites of hexagonal $YbMnO_3$. All values are based on the preliminary crystal field parameters reported by Diviš *et al* [8].

Yb site	a	b	c	$\langle J_z\rangle$	$\langle 3J_z^2 - J(J+1)\rangle$	g_z	$g_\perp$
2a	± 0.454	-0.647	∓ 0.613	1.007	2.235	2.302	3.597
4b	± 0.449	-0.630	∓ 0.634	1.099	3.096	2.512	3.555

with $B_2^0 = -4.1$ K, $B_4^0 = 15.5$ mK, $B_4^3 = -11.7$ K, $B_6^0 = 8.0$ mK, $B_6^3 = -53.7$ mK and $B_6^6 = 91.0$ mK for the 2a site and $B_2^0 = -6.6$ K, $B_4^0 = 18.0$ mK, $B_4^3 = -13.5$ K, $B_6^0 = 9.3$ mK, $B_6^3 = -61.9$ mK and $B_6^6 = 105.4$ mK for the 4b site. Diagonalization of the CF Hamiltonian yields, for each site, a CF scheme where the ground state is a well-isolated Kramers doublet of the form

$$|\pm\rangle = \pm a|\mp\tfrac{5}{2}\rangle - b|\pm\tfrac{1}{2}\rangle \mp c|\pm\tfrac{7}{2}\rangle \tag{3}$$

with coefficients, expectation values $\langle J_z\rangle$ and $\langle 3J_z^2 - J(J+1)\rangle$, and effective g-values as shown in table 3. The next excited Kramers doublets are at energies of at least 600 K and the maximum IR transition splitting of ≈30 cm^{-1} (or ≈44 K) observed by Diviš *et al* [8] is small by comparison. The spectrum analysis model of a well-isolated, fluctuating Kramers doublet is therefore clearly appropriate at the relatively low ^{170}Yb Mössbauer spectrum acquisition temperature of 4.5 K. As expected, the predicted ground state expectation values of $\langle J_z\rangle$ and $\langle 3J_z^2 - J(J+1)\rangle$ (refer to table 3) are significantly 'quenched' when compared with the free ion values of $J = 7/2$ and $3J^2 - J(J+1) = J(2J-1) = 21$, respectively.

If we persist with the interpretation that the 'static' component of the ^{170}Yb Mössbauer spectrum is associated with the Yb 4b site, then it is possible to arrive at a CF model estimate of the magnetic hyperfine field. The influence of a magnetic field on a Kramers doublet with effective spin $S = 1/2$ is described in the appendix of [25]. For the special case of a molecular field applied perpendicular to the c-axis, $\langle S_x\rangle = \pm 1/2$ and $\langle S_z\rangle = 0$. This means that

$$B_{\rm hf} = B_{\rm hf}(\text{free ion})\frac{\langle J_x\rangle}{J} = B_{\rm hf}(\text{free ion})\frac{g_\perp\langle S_x\rangle}{g_J J}. \tag{4}$$

Substitution of the CF model estimate of $g_\perp(4b) = 3.555$ (from table 3) and $g_J = 8/7$ for Yb^{3+} gives $B_{\rm hf} = 183.2$ T which is in close agreement with the fitted value of 173.5 T. CF model estimation of the quadrupole interaction strength is less reliable in the sense the total eQV_{zz} involves a summation of 4f shell and lattice contributions that are of opposite sign. Numerical solutions of the 4b site CF Hamiltonian with molecular field acting perpendicular to the c-axis indicate that the expectation value, $\langle 3J_z^2 - J(J+1)\rangle$, is only marginally affected. However some additional off-diagonal terms are introduced. If we ignore these for the moment, then

$$eQV_{zz}(\text{4f}) = eQV_{zz}(\text{free ion})\langle 3J_z^2 - J(J+1)\rangle / J(2J-1) \tag{5a}$$

and

$$eQV_{zz}(\text{latt}) = -4\frac{(1-\gamma_\infty)Q}{\theta_2(1-\sigma_2)\langle r^2\rangle_{\rm 4f}}B_2^0 \tag{5b}$$

where the various symbols have their usual meaning [24] and we arrive at an estimate of $eQV_{zz}(4b) \approx 3.5$ mm s^{-1}. This is with reference to the c-axis as the z-axis. Projection onto the direction of the induced $B_{\rm hf}$ (assumed to lie in the basal plane) gives $eQV_{z'z'} \approx -1.8$ mm s^{-1} which is close to the experimentally determined magnitude of 1.68(1) mm s^{-1} but is of opposite sign.

Finally, it is possible to say something about the Yb magnetic moments that are expected below the Yb sub-lattice ordering temperature of $T_{N_2} \approx 3$ K. If the moments lie in the basal plane, then the saturation moment associated with each Kramers doublet ground state is given by

$$\mu_{\rm sat}(\text{Yb}) = g_\perp\mu_{\rm B}\langle S_x\rangle. \tag{6}$$

Substitution of the CF model estimates of $g_\perp$ (from table 3) into equation (5) results in a saturation moment of ≈1.8 $\mu_{\rm B}$ averaged across the two Yb sites. This is in excellent agreement with the saturation magnetization of ≈1.6 $\mu_{\rm B}$/f.u. observed by Sugie *et al* [21] with an external field of 7 T applied perpendicular to the c-axis of a single-crystal h-$YbMnO_3$ specimen. It is evident from these considerations that the preliminary CF model proposed by Diviš *et al* [8] is already providing a useful description of the CF quenching process for the two Yb sites in h-$YbMnO_3$.

5. Conclusion

In conclusion, we have demonstrated that dilute concentrations of ^{57}Fe provide a useful Mössbauer spectroscopy probe of the Mn sub-lattice magnetization in hexagonal phase rare earth manganites. In the present case of h-$YbMnO_3$, substitution of up to 1 at.% ^{57}Fe for Mn exerts negligible influence on the Néel temperature and point charge model estimates of the electric field gradient agree well with experimental ^{57}Fe Mössbauer results in terms of both sign and magnitude. The ^{170}Yb Mössbauer spectrum recorded at 4.5 K is in keeping with a fluctuating, well-isolated, Kramers doublet ground state at both sites. The 'static', five-line sub-spectrum is proposed to correspond to the 4b site and the preliminary CF model proposed by Diviš *et al* [8] is demonstrated to provide a useful description of the strong CF quenching.

Acknowledgments

M Powell and N Browne are acknowledged for their assistance with the preparation of the ^{57}Fe-doped specimens. HAS gratefully acknowledges her University International Postgraduate Award and University College Postgraduate Research Scholarship. The ^{170}Yb source activations were carried out by M Butler at the McMaster Nuclear Reactor (MNR), Hamilton, Ontario.

References

[1] Isobe M, Kimizuka N, Nakamura M and Mohri T 1991 *Acta Crystallogr.* C **47** 423–4

[2] van Aken B B, Meetsma A and Palstra T T M 2001 *Acta Crystallogr.* E **57** i87–9

[3] van Aken B B, Meetsma A and Palstra T T M 2001 *Preprint* cond-mat/0106298

[4] Park J, Park J-G, Jeon G S, Choi H Y, Lee C, Jo W, Bewley R, McEwen K A and Perring T G 2003 *Phys. Rev.* B **68** 104426

[5] Katsufuji T, Mori S, Masaki M, Moritomo Y, Yamamoto N and Takagi H 2001 *Phys. Rev.* B **64** 104419

[6] Yoshii K and Abe H 2002 *J. Solid State Chem.* **165** 131–5

[7] Huang Y H, Fjellvåg H, Karppinen M, Hauback B C, Yamauchi H and Goodenough J B 2006 *Chem. Mater.* **18** 2130–4

[8] Diviš M, Hölsä J, Lastusaari M, Litvinchuk A P and Nekvasil V 2008 *J. Alloys Compounds* **451** 662–5

[9] Howard C J and Hunter B A 2000 Rietica available from http://www.ccp14.ac.uk.

[10] Zhou J-S, Goodenough J B, Gallardo-Amores J M, Morán E, Alario-Franco M A and Caudillo R 2006 *Phys. Rev.* B **74** 014422

[11] Stewart G A, McPherson I M, Gubbens P C M, Kaiser C T, Dalmas de Réotier P, Yaouanc A and Cottrell S P 2003 *J. Alloys Compounds* **358** 7–11

[12] Stewart G A, McPherson I M, Harker S J and Edge A V J 2005 *Proc. 16th Australian Institute of Physics Congr. (Canberra)* http://aipcongress2005.anu.edu.au/pdf/PAPERS-2.pdf

[13] Bocquet S, Pollard R J and Cashion J D 1992 *Phys. Rev.* B **46** 11657

[14] Bocquet S and De Grave E 1994 *J. Phys.: Condens. Matter* **6** 6825

[15] Park J, Kong U, Pirogov A, Choi S I, Park J-G, Choi Y N, Lee C and Jo W 2002 *Appl. Phys.* A **74** S796–8
Lee S and Park J G 2006 *Neutron News* **173** 24–7

[16] Munoz A, Alonso J A, Martinez-Lope M J, Casais M T, Martinez J L and Fernandez-Diaz M T 2000 *Phys. Rev.* B **62** 9498–510

[17] Lonkai T 2004 *Thesis* Eberhard-Karls-Universität Tübingen

[18] Stewart G A 1994 *Mater. Forum* **18** 177–93

[19] Hodges J A, Bonville P, Forget A, Yaouanc A, Dalmas der Reotier P, Andre G, Rams M, Krolas K, Ritter C, Gubbens P C M, Kaiser C T, King P J C and Baines C 2002 *Phys. Rev. Lett.* **88** 077204

[20] Wickmann H H, Klein M P and Shirley D A 1966 *Phys. Rev.* **152** 345–57

[21] Sugie H, Iwata N and Kohn K 2002 *J. Phys. Soc. Japan* **71** 1558–64

[22] Shannon R D 1978 *Acta Crystallogr.* A **32** 751–67

[23] Fiebig M, Fröhlich D, Kohn K, Leute St, Lottermoser Th, Pavlov V V and Pisarev R V 2000 *Phys. Rev. Lett.* **84** 5620

[24] Stewart G A 1985 *Hyperfine Interact.* **23** 1–16

[25] Bonville P, Hodges J A, Imbert P and Hartmann-Boutron F 1978 *Phys. Rev.* B **18** 2196–208